Progress In Electromagnetics Research B, Vol. 26, 237–256, 2010

VECTORIAL STRUCTURE OF A PHASE-FLIPPED GAUSS BEAM IN THE FAR FIELD

J. Li, Y. R. Chen, S. X. Xu, Y. Q. Wang, M. C. Zhou Q. Zhao, Y. Xin, and F. N. Chen

Department of Optical Engineering
Nanjing University of Science and Technology
Jiangsu, Nanjing 210094, China

Abstract—Based on the vectorial angular spectrum representation and the method of stationary phase, internal vectorial structures of a phase-flipped Gauss (PFG) beam diffracting in the far field are derived in analytical forms. The energy flux for the TE term, TM term and the whole beam are derived and depicted by numerical examples. Influences of the f parameter on the whole energy flux distributions are analyzed. Discrepancies of the whole energy flux distributions between the paraxial and non-paraxial cases are shown in detailed manners. Furthermore, influences of the f parameter on discrepancies between two cases are also studied.

1. INTRODUCTION

In has been known for a long time that, although most single-mode laser sources, such as the TEM_{00} Gaussian mode as well as its standard output beam, have been widely utilized in various experimental aspects. However, generally speaking, it requires very strict to beam profiles in applications such as high precise optical measurements and laser beam shaping. Based on these facts, it has been demonstrated that some special beam profiles are required to improve the efficiency in applications of optical measurements. Very recently, a novel optical technique that the generation of a TEM_{00} Gaussian beam which owns a π phase flip between two halves of the beam profile is proposed. It has been presented that such beams can be generated by utilizing a special wave plate and a masked Sagnac interferometer [1]. The phase-flipped Gaussian (PFG)

Received 25 August 2010, Accepted 13 October 2010, Scheduled 22 October 2010
Corresponding author: Jia Li (lijiafeifei@sina.com).

beam has been shown to have potential applications in high precise resolution measurements within one dimensional spatial domain. Since then, N. Treps et al. demonstrated the experimental method for the displacement measurement by utilizing multimode squeezed light within internal phase flips, in order to surpass the standard quantum limit [2]. Subsequently, based on the Huygens-Fresnel diffraction integral and decompositions of the flipped mode into infinite sum of odd Hermite-Gaussian modes, the closed-form analytical expressions for a PFG beam are derived and its propagation properties through a paraxial ABCD optical system have been known [3]. The non-paraxial diffraction properties of a linearly polarized PFG beam have been studied by using the Rayleigh-Sommerfeld diffraction integral [4]. Furthermore, an extended work has been made to reveal the recurrence propagation expressions for the multi-mode Hermite-Gaussian beams with a π phase flip between two halves of the beam profile [5]. It has been indicated that the propagation of the PFG beam should be treated as a special case of that of the phase-flipped Hermite-Gaussian beams. On the other hand, the internal vectorial structures of laser beams have attracted much attention. It has been proved that, for an arbitrary polarized electromagnetic beam, which can be expressed in terms of vectorial angular spectrum, is approximately composed of the transversal electric (TE) term and the transversal magnetic (TM) term [6–8]. Many investigations have been carried out dealing with vectorial structural characteristics of various laser beams in the far field [9–18], by means of the method of stationary phase [19, 20]. Based on these studies, a question may arise: what impact would a π flip phase have on the TE term, TM term and the whole beam in the far field? However, to the best of our knowledge, there has been no report conducting the investigation of the internal vectorial structure of the PFG beam in the far field. Due to above statements, this paper is aim to reveal the characteristics for the internal structures of the PFG beam. The far-field energy flux distributions of a linearly polarized vectorial PFG beam are expressed and corresponding results are illustrated by numerical examples. Subsequently, influences of the f parameter on the whole energy flux distributions are analyzed. Discrepancies of the whole energy flux distributions between the paraxial and non-paraxial cases are shown in detailed manners. Finally, the influence of the f parameter on these discrepancies is also investigated. Some comparisons are also made, in order to show behaviors of the PFG beam in a much detailed manner.

2. ANALYTICAL EXPRESSIONS FOR THE FAR-FIELD TE AND TM TERMS

At the initial plane $z = 0$, assuming that the electric field of a PFG beam is linearly polarized along the x direction in the two-dimensional transversal Cartesian coordinate system, which takes the following analytical form [1–5]

$$E(x_0, y_0, 0) = \theta(x_0)\,\theta(y_0)\,E_0(x_0, y_0, 0)\,\hat{\mathbf{e}}_x, \tag{1}$$

With

$$\theta(x_0) = \begin{cases} -1 & x_0 < 0, \\ 1 & x_0 \geq 0, \end{cases} \qquad \theta(y_0) = \begin{cases} -1 & y_0 < 0, \\ 1 & y_0 \geq 0, \end{cases} \tag{2}$$

$$E_0(x_0, y_0, 0) = \frac{\sqrt{2/\pi}}{w_0} \exp\left(-\frac{x_0^2 + y_0^2}{w_0^2}\right), \tag{3}$$

where w_0 denotes the waist width of the Gaussian beam at the plane $z = 0$, $\hat{\mathbf{e}}_x$ is the unit vector along the x direction. $\frac{\sqrt{2/\pi}}{w_0}$ is the normalized factor whose action is to retain invariant laser powers at the plane $z = 0$. Fig. 1 shows the amplitude of the electric field component $E(x_0, y_0, 0)$ in the transversal plane $z = 0$. It can be observed that, at the axis line $x = 0$ or $y = 0$, there exists a π phase flip. As a result, the amplitude of the electric field takes rapid transitions. The similar phenomenon of the PFG beam can also be observed from Fig. 1 of Ref. [1, 3].

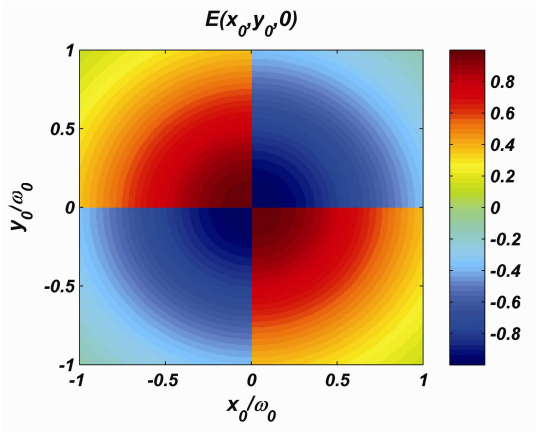

Figure 1. Contour plots for amplitude of the electric field $E(x_0, y_0, 0)$ of the PFG beam within π flip phase at $x = 0$ and $y = 0$.

Based on the vectorial angular representation of the Maxwell's equations, the diffracted electric field in the half space $z > 0$ turns out to be [6–8]

$$E(\hat{\mathbf{r}}) = \int_{-\infty}^{+\infty} \int_{-\infty}^{+\infty} A(p,q,m) \exp[ik(px + qy + mz)]\, dpdq, \tag{4}$$

With

$$A(p,q,m) = A_x(p,q)\left(\hat{\mathbf{i}} - \frac{p}{m}\hat{\mathbf{k}}\right), \tag{5}$$

$$m = \begin{cases} \left(1 - p^2 - q^2\right)^{1/2} & p^2 + q^2 \le 1 \\ i\left(p^2 + q^2 - 1\right)^{1/2} & p^2 + q^2 > 1 \end{cases}, \tag{6}$$

where $\hat{\mathbf{r}} = x\hat{\mathbf{i}} + y\hat{\mathbf{j}} + z\hat{\mathbf{k}}$ is the positional vector in the output plane, k is the wave number which is related with the wavelength as $k = 2\pi/\lambda$. The main result of this paper is based on Eq. (5), the vectorial angular spectrum representation of an arbitrary electromagnetic wave on a given plane.This result is an approximation which is only suitable for the far-field region of electromagnetic beams, of which effects of the evanescent wave can be neglected. Whereas, in the near diffraction field, effects of the evanescent wave should be considered, the method of the vectorial angular spectrum used in this paper can not be applicable anymore. In this situation, a more rigorous approach, i.e., the disposal based on vector potentials of electromagnetic Hertz vector, can be performed. This method shows little precision than the method of vectorial angular spectrum utilized in this paper, because the weight of the evanescent wave is so trivial compared to that of the homogeneous one, in general. In a word, the method of the vectorial angular spectrum is not only precise in calculations here but also shows explicit in its final analytical form. Eq. (6) indicates that the inequality $p^2 + q^2 \le 1$ corresponds to the homogeneous wave on diffraction. Comparably, the inequality $p^2 + q^2 > 1$ corresponds to the diffraction of the evanescent wave. p and q are two orthogonal components defined in the frequency domain. In Eq. (5), the component $Ax(p,q)$ can be determined by the Fourier transformation of the x component of the initial electric field [9–18]

$$A_x(p,q) = \frac{1}{\lambda^2} \int_{-\infty}^{+\infty} \int_{-\infty}^{+\infty} E_x(x_0, y_0, 0) \exp[-ik(px_0 + qy_0)]\, dx_0 dy_0, \tag{7}$$

Noted that in Eqs. (4) and (7), the time-dependent factor $\exp(-i\omega t)$ is omitted, in which ω denotes the angular frequency. Eq. (4) means that, during the diffraction of beams in free space, the longitudinal electric field component may arise which results from the divergence

theorem of the electric field [20]. In the far-field transversal plane, the TE and TM terms are perpendicular to each other. Based on these facts, in the frequency domain, there exist two unit vectors $\hat{\mathbf{e}}_1$ and $\hat{\mathbf{e}}_2$ which can be defined as [6–8]

$$\hat{\mathbf{e}}_1 = \frac{q}{(p^2+q^2)^{1/2}}\hat{\mathbf{e}}_x - \frac{p}{(p^2+q^2)^{1/2}}\hat{\mathbf{e}}_y, \tag{8a}$$

$$\hat{\mathbf{e}}_2 = \frac{pm}{(p^2+q^2)^{1/2}}\hat{\mathbf{e}}_x + \frac{qm}{(p^2+q^2)^{1/2}}\hat{\mathbf{e}}_y - \left(p^2+q^2\right)^{1/2}\hat{\mathbf{e}}_z, \tag{8b}$$

where $\hat{\mathbf{e}}_y$ and $\hat{\mathbf{e}}_z$ are the unit vectors along the y and z directions defined in the three dimensional Cartesian coordinate system. Then three unit vectors $\hat{\mathbf{s}}$, $\hat{\mathbf{e}}_1$, $\hat{\mathbf{e}}_2$ should form a mutually perpendicular right-handed system

$$\hat{\mathbf{s}} \times \hat{\mathbf{e}}_1 = \hat{\mathbf{e}}_2, \quad \hat{\mathbf{e}}_1 \times \hat{\mathbf{e}}_2 = \hat{\mathbf{s}}, \quad \hat{\mathbf{e}}_2 \times \hat{\mathbf{s}} = \hat{\mathbf{e}}_1, \tag{9}$$

where $\hat{\mathbf{s}} = p\hat{\mathbf{e}}_x + q\hat{\mathbf{e}}_y + m\hat{\mathbf{e}}_z$. According to Eqs. (8) and (9), in the far-field region, the diffracted electric field can be expressed as a sum of the TE and TM terms [9–15]

$$E(\hat{\mathbf{r}}) = E_{\mathrm{TE}}(\hat{\mathbf{r}}) + E_{\mathrm{TM}}(\hat{\mathbf{r}}), \tag{10}$$

with $E_{\mathrm{TE}}(\hat{\mathbf{r}})$ and $E_{\mathrm{TM}}(\hat{\mathbf{r}})$ given by

$$E_{\mathrm{TE}}(\hat{\mathbf{r}}) = \int_{-\infty}^{+\infty}\int_{-\infty}^{+\infty}[A(p,q)\cdot\hat{\mathbf{e}}_1]\hat{\mathbf{e}}_1 \times \exp[ik(px+qy+mz)]dpdq, \tag{11a}$$

$$E_{\mathrm{TM}}(\hat{\mathbf{r}}) = \int_{-\infty}^{+\infty}\int_{-\infty}^{+\infty}[A(p,q)\cdot\hat{\mathbf{e}}_2]\,\hat{\mathbf{e}}_2 \times \exp[ik(px+qy+mz)]dpdq, \tag{11b}$$

Similarly, the diffracted magnetic field can also be expressed as a sum of the TE and TM terms

$$H(\hat{\mathbf{r}}) = H_{\mathrm{TE}}(\hat{\mathbf{r}}) + H_{\mathrm{TM}}(\hat{\mathbf{r}}), \tag{12}$$

with $H_{\mathrm{TE}}(\hat{\mathbf{r}})$ and $H_{\mathrm{TM}}(\hat{\mathbf{r}})$ given by

$$H_{\mathrm{TE}}(\hat{\mathbf{r}}) = \int_{-\infty}^{+\infty}\int_{-\infty}^{+\infty}[A(p,q)\cdot\hat{\mathbf{e}}_1]\,\hat{\mathbf{e}}_2 \times \exp[ik(px+qy+mz)]dpdq, \tag{13a}$$

$$H_{\mathrm{TM}}(\hat{\mathbf{r}}) = \int_{-\infty}^{+\infty}\int_{-\infty}^{+\infty}[A(p,q)\cdot\hat{\mathbf{e}}_2]\,\hat{\mathbf{e}}_1 \times \exp[ik(px+qy+mz)]dpdq, \tag{13b}$$

Substituting Eqs. (1)–(3) into Eq. (7), the vectorial angular spectrum

component $Ax(p,q)$ can be expressed as

$$A_x(p,q) = \frac{\sqrt{2/\pi}}{w_0}\int_{-\infty}^{+\infty}\theta(x_0)\exp\left(-\frac{x_0^2}{w_0^2}-ikpx_0\right)dx_0\int_{-\infty}^{+\infty}\theta(y_0)$$
$$\exp\left(-\frac{y_0^2}{w_0^2}-ikqy_0\right)dy_0 = \frac{\sqrt{2/\pi}}{w_0}\left\{\int_0^{+\infty}\exp\left(-\frac{x_0^2}{w_0^2}-ikpx_0\right)dx_0\right.$$
$$\left.-\int_0^{+\infty}\exp\left(-\frac{x_0^2}{w_0^2}+ikpx_0\right)dx_0\right\}\times\left\{\int_0^{+\infty}\exp\left(-\frac{y_0^2}{w_0^2}-ikqy_0\right)dy_0\right.$$
$$\left.-\int_0^{+\infty}\exp\left(-\frac{y_0^2}{w_0^2}+ikqy_0\right)dy_0\right\}, \tag{14}$$

Recalling the following integral formula [21]

$$\int_0^{+\infty}\exp\left(-\frac{x^2}{4\beta}-\gamma x\right)dx = \sqrt{\pi\beta}\exp\left(\beta\gamma^2\right)\left\{1-\mathrm{erf}\left(\gamma\sqrt{\beta}\right)\right\},$$
$$\mathrm{Re}\,\beta > 0, \tag{15}$$

After tedious but straightforward integral calculations, Eq. (14) can be further arranged into the following analytical form

$$A_x(p,q) = \frac{1}{4\sqrt{2\pi}\lambda f}\exp\left\{-\frac{1}{4f^2}\left(p^2+q^2\right)\right\}\left\{\mathrm{erf}\left(-\frac{i}{2f}p\right)-\mathrm{erf}\left(\frac{i}{2f}p\right)\right\}$$
$$\times\left\{\mathrm{erf}\left(-\frac{i}{2f}q\right)-\mathrm{erf}\left(\frac{i}{2f}q\right)\right\}, \tag{16}$$

where the sign "erf" denotes the error function. $f = 1/kw_0$ is the f parameter which has been defined in [4, 5]. In general, the f parameter is commonly utilized to describe how paraxial degree of a laser beam evaluates, upon propagation. Subsequently, substituting Eqs. (5) and (16) into Eq. (11), after tedious vectorial performances, the diffracted electric field for the TE and TM terms can be further rewritten as

$$E_{\mathrm{TE}}(\hat{\mathbf{r}}) = \frac{1}{4\sqrt{2\pi}\lambda f}\int_{-\infty}^{+\infty}\int_{-\infty}^{+\infty}\exp\left\{-\frac{1}{4f^2}\left(p^2+q^2\right)\right\}\left\{\mathrm{erf}\left(-\frac{i}{2f}p\right)\right.$$
$$\left.-\mathrm{erf}\left(\frac{i}{2f}p\right)\right\}\times\left\{\mathrm{erf}\left(-\frac{i}{2f}q\right)-\mathrm{erf}\left(\frac{i}{2f}q\right)\right\}\frac{q}{p^2+q^2}\left(q\hat{\mathbf{e}}_x-p\hat{\mathbf{e}}_y\right)$$
$$\times\exp[ik(px+qy+mz)]\,dpdq, \tag{17a}$$

$$E_{\mathrm{TM}}(\hat{\mathbf{r}}) = \frac{1}{4\sqrt{2\pi}\lambda f}\int_{-\infty}^{+\infty}\int_{-\infty}^{+\infty}\exp\left\{-\frac{1}{4f^2}\left(p^2+q^2\right)\right\}\left\{\mathrm{erf}\left(-\frac{i}{2f}p\right)\right.$$
$$\left.-\mathrm{erf}\left(\frac{i}{2f}p\right)\right\}\times\left\{\mathrm{erf}\left(-\frac{i}{2f}q\right)-\mathrm{erf}\left(\frac{i}{2f}q\right)\right\}\left(\frac{p^2}{p^2+q^2}\hat{\mathbf{e}}_x+\frac{pq}{p^2+q^2}\hat{\mathbf{e}}_y\right.$$
$$\left.-\frac{p}{m}\hat{\mathbf{e}}_z\right)\times\exp[ik(px+qy+mz)]\,dpdq, \tag{17b}$$

Similarly, Substituting Eqs. (5) and (16) into Eq. (13), the diffracted magnetic field for the TE and TM terms can be expressed as

$$H_{\mathrm{TE}}(\hat{\mathbf{r}}) = \frac{1}{4\sqrt{2\pi}\lambda f}\int_{-\infty}^{+\infty}\int_{-\infty}^{+\infty}\exp\left\{-\frac{1}{4f^2}\left(p^2+q^2\right)\right\}\left\{\mathrm{erf}\left(-\frac{i}{2f}p\right)\right.$$
$$\left.-\mathrm{erf}\left(\frac{i}{2f}p\right)\right\}\times\left\{\mathrm{erf}\left(-\frac{i}{2f}q\right)-\mathrm{erf}\left(\frac{i}{2f}q\right)\right\}\frac{q}{p^2+q^2}\left\{pm\hat{\mathbf{e}}_x+qm\hat{\mathbf{e}}_y\right.$$
$$\left.-\left(p^2+q^2\right)\hat{\mathbf{e}}_z\right\}\times\exp[ik\left(px+qy+mz\right)]\,dpdq, \tag{18a}$$

$$H_{\mathrm{TM}}(\hat{\mathbf{r}}) = \frac{1}{4\sqrt{2\pi}\lambda f}\int_{-\infty}^{+\infty}\int_{-\infty}^{+\infty}\exp\left\{-\frac{1}{4f^2}\left(p^2+q^2\right)\right\}\left\{\mathrm{erf}\left(-\frac{i}{2f}p\right)\right.$$
$$\left.-\mathrm{erf}\left(\frac{i}{2f}p\right)\right\}\times\left\{\mathrm{erf}\left(-\frac{i}{2f}q\right)-\mathrm{erf}\left(\frac{i}{2f}q\right)\right\}\frac{p}{\left(p^2+q^2\right)m}\left(q\hat{\mathbf{e}}_x-p\hat{\mathbf{e}}_y\right)$$
$$\times\exp[ik\left(px+qy+mz\right)]\,dpdq, \tag{18b}$$

For the diffraction of the PFG beam in the far field, integrations in Eqs. (17) and (18) can be performed by utilizing the method of stationary phase [19, 20]. In this paper, the utilization of this method indicates that, the integrals in Eqs. (17) and (18) should be restricted within the range of $0 \le p^2+q^2 \le 1$. Therefore, in the following derivations, the condition $kr = k(x^2+y^2+z^2)^{1/2} \to \infty$ is fulfilled. After tedious integral calculations, the electric and magnetic field components for the TE and TM terms can be respectively derived as

$$E_{\mathrm{TE}}(\hat{\mathbf{r}}) = -i\frac{yz}{4\sqrt{2\pi}f\rho^2r^2}\exp\left(-\frac{\rho^2}{4f^2r^2}\right)\left\{\mathrm{erf}\left(-\frac{i}{2fr}x\right)-\mathrm{erf}\left(\frac{i}{2fr}x\right)\right\}$$
$$\left\{\mathrm{erf}\left(-\frac{i}{2fr}y\right)-\mathrm{erf}\left(\frac{i}{2fr}y\right)\right\}\times\left(y\hat{\mathbf{e}}_x-x\hat{\mathbf{e}}_y\right)\exp(ikr)\,, \tag{19a}$$

$$E_{\mathrm{TM}}(\hat{\mathbf{r}}) = -i\frac{x}{4\sqrt{2\pi}f\rho^2r^2}\exp\left(-\frac{\rho^2}{4f^2r^2}\right)\left\{\mathrm{erf}\left(-\frac{i}{2fr}x\right)-\mathrm{erf}\left(\frac{i}{2fr}x\right)\right\}$$
$$\left\{\mathrm{erf}\left(-\frac{i}{2fr}y\right)-\mathrm{erf}\left(\frac{i}{2fr}y\right)\right\}\times\left(xz\hat{\mathbf{e}}_x+yz\hat{\mathbf{e}}_y-\rho^2\hat{\mathbf{e}}_z\right)\exp(ikr)\,, \tag{19b}$$

$$H_{\mathrm{TE}}(\hat{\mathbf{r}}) = -i\frac{yz}{4\sqrt{2\pi}f\rho^2r^3}\left(\varepsilon_0/\mu_0\right)^{1/2}\exp\left(-\frac{\rho^2}{4f^2r^2}\right)\left\{\mathrm{erf}\left(-\frac{i}{2fr}x\right)\right.$$
$$\left.-\mathrm{erf}\left(\frac{i}{2fr}x\right)\right\}\times\left\{\mathrm{erf}\left(-\frac{i}{2fr}y\right)-\mathrm{erf}\left(\frac{i}{2fr}y\right)\right\}$$
$$\left(xz\hat{\mathbf{e}}_x+yz\hat{\mathbf{e}}_y-\rho^2\hat{\mathbf{e}}_z\right)\exp(ikr)\,, \tag{19c}$$

$$H_{\mathrm{TM}}(\hat{\mathbf{r}}) = i\frac{x}{4\sqrt{2\pi}f\rho^2 r}(\varepsilon_0/\mu_0)^{1/2}\exp\left(-\frac{\rho^2}{4f^2r^2}\right)\left\{\mathrm{erf}\left(-\frac{i}{2fr}x\right)\right.$$
$$\left.-\mathrm{erf}\left(\frac{i}{2fr}x\right)\right\}\times\left\{\mathrm{erf}\left(-\frac{i}{2fr}y\right)-\mathrm{erf}\left(\frac{i}{2fr}y\right)\right\}(y\hat{\mathbf{e}}_x - x\hat{\mathbf{e}}_y)\exp(ikr), \quad (19d)$$

where $r = (x^2+y^2+z^2)^{1/2}$, $\rho = (x^2+y^2)^{1/2}$. ε_0 and μ_0 are the electric permittivity and the magnetic permeability of vacuum, respectively. Observing from Eq. (19), it is found that, in the far field region, the TE and TM terms for both the electric and magnetic fields are orthogonal to each other. On the other hand, analytical forms such as Eqs. (18) and (19) are based on the validity of the vectorial angular spectrum representation, since the range of the f parameter has not been limited, the analytical TE and TM terms of the PFG beam are applicable not only to the paraxial case, but also to the non-paraxial case.

3. ENERGY FLUX DISTRIBUTIONS OF THE PFG BEAM IN THE FAR FIELD

As the non-paraxial case should be taken into considerations, in order to study the characteristics of the PFG beam in the far field, the intensity distributions should be replaced by the energy flux distributions. The energy flux distribution is defined by the z component of the time-average Poynting vector

$$\langle S_z\rangle = \frac{1}{2}\mathrm{Re}\left[E(\hat{\mathbf{r}})\times H^*(\hat{\mathbf{r}})\right]_z, \quad (20)$$

where Re denotes taking the real part and the asterisk means the complex conjugation. The angle bracket indicates taking the ensemble average with respect to the time variable t. Accordingly, the energy flux distributions of TE and TM terms in the far field are respectively given by

$$\langle S_z\rangle_{\mathrm{TE}} = \frac{1}{2}Re\left[E_{\mathrm{TE}}(\hat{\mathbf{r}})\times H^*_{\mathrm{TE}}(\hat{\mathbf{r}})\right]_z$$
$$= \frac{y^2z^3}{32\pi f^2\rho^2 r^5}(\varepsilon_0/\mu_0)^{1/2}\exp\left(-\frac{\rho^2}{2f^2r^2}\right)\times\left|\mathrm{erf}\left(-\frac{i}{2fr}x\right)-\mathrm{erf}\left(\frac{i}{2fr}x\right)\right|^2$$
$$\times\left|\mathrm{erf}\left(-\frac{i}{2fr}y\right)-\mathrm{erf}\left(\frac{i}{2fr}y\right)\right|^2, \quad (21)$$

$$\langle S_z\rangle_{\mathrm{TM}} = \frac{1}{2} Re\left[E_{\mathrm{TM}}(\hat{\mathbf{r}}) \times H^*_{\mathrm{TM}}(\hat{\mathbf{r}})\right]_z$$
$$= \frac{x^2 z}{32\pi f^2 \rho^2 r^3} (\varepsilon_0/\mu_0)^{1/2} \exp\left(-\frac{\rho^2}{2f^2 r^2}\right) \times \left|\mathrm{erf}\left(-\frac{i}{2fr}x\right) - \mathrm{erf}\left(\frac{i}{2fr}x\right)\right|^2$$
$$\times \left|\mathrm{erf}\left(-\frac{i}{2fr}y\right) - \mathrm{erf}\left(\frac{i}{2fr}y\right)\right|^2, \tag{22}$$

The total energy flux distribution of the PFG beam yields

$$\langle S_z\rangle = \langle S_z\rangle_{\mathrm{TE}} + \langle S_z\rangle_{\mathrm{TM}}$$
$$= \frac{z}{32\pi f^2 \rho^2 r^3}\left(x^2 + \frac{z^2}{r^2}y^2\right)\exp\left(-\frac{\rho^2}{2f^2 r^2}\right) \times \left|\mathrm{erf}\left(-\frac{i}{2fr}x\right) - \mathrm{erf}\left(\frac{i}{2fr}x\right)\right|^2$$
$$\times \left|\mathrm{erf}\left(-\frac{i}{2fr}y\right) - \mathrm{erf}\left(\frac{i}{2fr}y\right)\right|^2, \tag{23}$$

Noted that Eqs. (21)–(23) are applicable for the general non-paraxial case of the PFG beam in the far field region. Some more special cases can be extracted from these analytical forms. In the paraxial case, the following approximation can be made [20]

$$r \approx z + \frac{\rho^2}{2z} \approx z, \tag{24}$$

Substituting Eq. (24) into Eq. (23), the total energy flux distribution for the paraxial case reduces to the form

$$\langle S_z\rangle_p = \frac{1}{32\pi f^2 \rho^2 z^2} \exp\left(-\frac{\rho^2}{2f^2 z^2}\right) \left|\mathrm{erf}\left(-\frac{i}{2fz}x\right) - \mathrm{erf}\left(\frac{i}{2fz}x\right)\right|^2$$
$$\times \left|\mathrm{erf}\left(-\frac{i}{2fz}y\right) - \mathrm{erf}\left(\frac{i}{2fz}y\right)\right|^2, \tag{25}$$

It should be pointed out that, the result of Eq. (25) is derived from Eq. (23), under the paraxial approximation (see Eq. (24)). Generally speaking, the method of stationary phase utilized in calculating the integrals in Eq. (17) and Eq. (18) can be applicable to both the paraxial and non-paraxial cases [19, 20], in the far-field region. Therefore, the analytical form of Eq. (23) stands for the energy flux distribution of the beam for both the paraxial and non-paraxial cases. On the other hand, Eq. (24) is also only valid in the far region; this is the same as the application of the method of stationary phase before. However, the paraxial approximation should be further required to the result of Eqs. (24) and (25), which indicates that the non-paraxial case can not be applicable to Eq. (25) anymore. In a word, these two approximations used in solving Eq. (17) and that of Eq. (24) are totally

different, because the latter one only applies to the paraxial case, comparably the former one can be applicable for both the paraxial and non-paraxial cases. For these two approximations, their differences can be further compared in Figs. 6, 7 as values of the f-parameter increase. This phenomenon would be elaborated in detail, in the next section below. Observing from Eqs. (21)–(25), one can conclude that, for the PFG beam diffracting into the far field, the energy flux distributions for the TE term, TM term and the whole beam would compose of a fundamental Gauss function and absolute values of the error functions. Comparing these analytical forms with previous ones [3–5], it demonstrates that the error functions shown in Eqs. (21)–(25) are induced by the π flip phase of the initial laser beam. This means that the far-field beam profile is affected by the flip phase of laser sources, which have an additional impact on diffraction patterns other than roles of Gauss functions. In the following part, some numerical simulations are performed to reveal the influence of the π flip phase of sources on the far-field energy flux distributions.

4. NUMERICAL EXAMPLES

Firstly, the energy flux distributions of the TE term, TM term and the whole PFG beam are depicted in Figs. 2–4, for different values of the f parameter. It has been known from previous reports [4, 5, 22] that, a PFG beam within larger f parameter may show more non-paraxial characteristics. To define a paraxial Gaussian beam, namely, $f \leq 0.18$ should be required at the plane $z = 0$ [22]. It is also found that, for a PFG beam diffracting in free space, the paraxial approximation holds true if $f \leq 0.04$ [4]. Figs. 2–4 show the energy flux distributions of the TE term, TM term and the whole PFG beam at the plane $z = 500\lambda$, while the f parameter is chosen as 0.32, 0.16, 0.03, respectively. A common phenomenon observed from these contour figures is that, after diffraction in free space for long distances, energy flux distributed profiles of the PFG beam would split into four separate side-lobes within axial shadows along the x and y axis. Causes for this phenomenon might be explained like this: The PFG beam carries π flipped phases at the cross line $x = 0$ and $y = 0$ of the plane $z = 0$ (see Fig. 1). The π flipped phase may cause discrepant properties between several parts of the PFG beam when it diffracts in free space. As a result, it may induce the discontinuity or even singularity of energy flux distributions. In another point of view, this phenomenon can also be explained in the analytical approach. In the vicinity of the axis $x = 0$ and $y = 0$, the error function in Eqs. (23) and (25) can be

approximately expressed as [4, 21]

$$\mathrm{erf}(x) = \frac{2x}{\sqrt{\pi}} + O\left(x^3\right), \quad \text{for } |x| \to 0, \tag{26}$$

within the approximation of Eq. (26), Eqs. (23) and (25) can be respectively rewritten as

$$\langle S_z \rangle = \frac{x^2 y^2 z}{2\pi^3 f^6 \rho^2 r^7} \left(x^2 + \frac{z^2}{r^2} y^2\right) \exp\left(-\frac{\rho^2}{2f^2 r^2}\right), \tag{27}$$

$$\langle S_z \rangle_p = \frac{x^2 y^2}{2\pi^3 f^6 z^6} \exp\left(-\frac{\rho^2}{2f^2 z^2}\right), \tag{28}$$

If $|x| \to 0$ or $|y| \to 0$ is satisfied in Eqs. (27) and (28), the energy flux distributions for both the paraxial and non-paraxial cases tend to zero. This is why the axial shadows occur in Figs. 2–4.

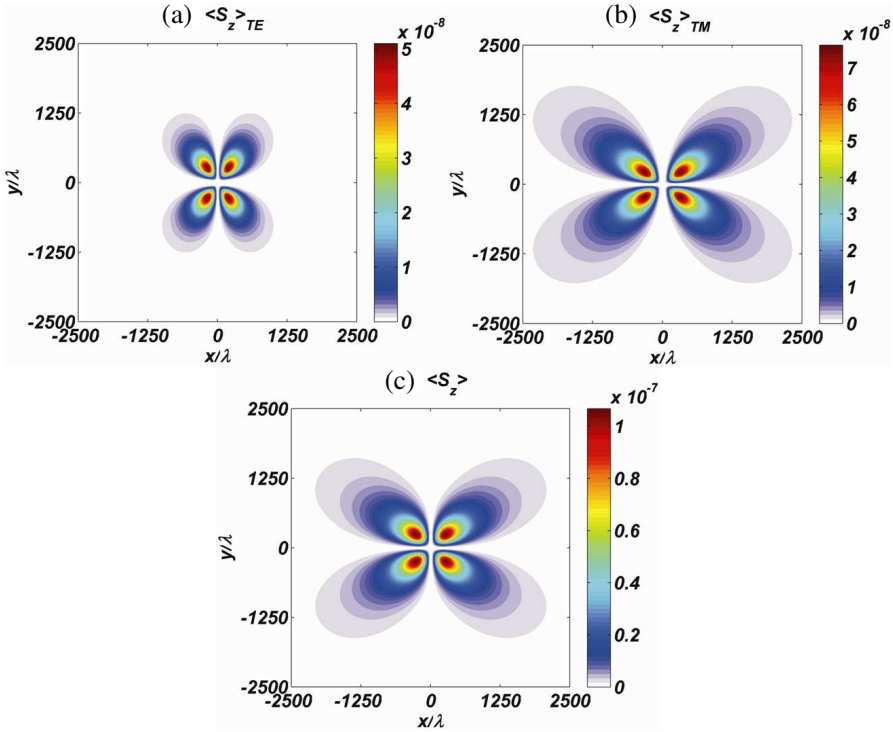

Figure 2. Energy flux distributions of the PFG beam at the plane $z = 500\lambda$, beam parameter $f = 0.32$. (a) TE term. (b) TM term. (c) The whole beam.

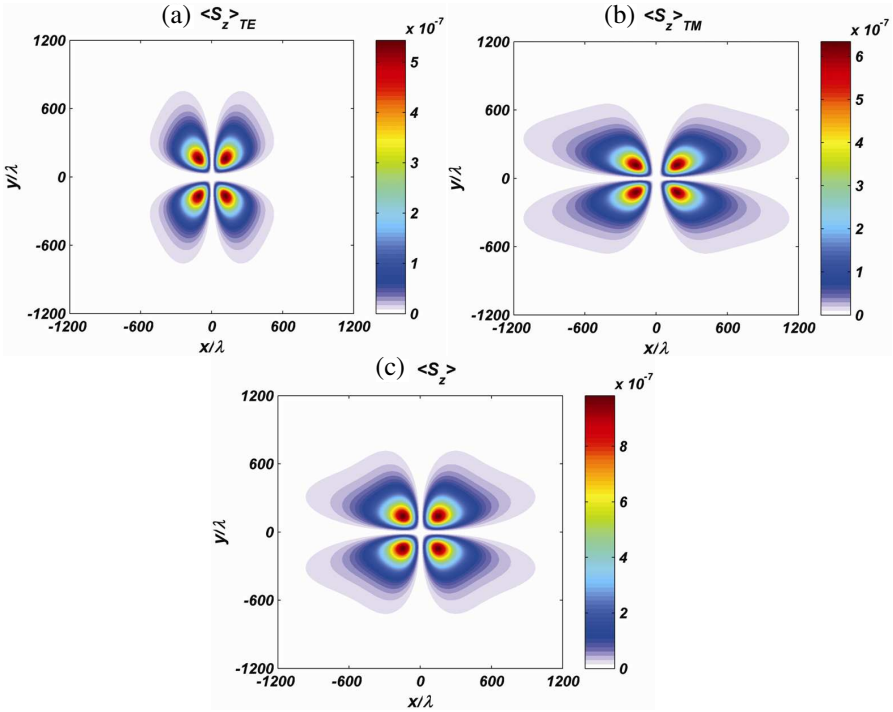

Figure 3. Energy flux distributions of the PFG beam at the plane $z = 500\lambda$, beam parameter $f = 0.16$. (a) TE term. (b) TM term. (c) The whole beam.

Secondly, one can observe that the energy flux distributions show discrepancies in their profiles, for different values of the f parameter. When $f = 0.32$, edges of profiles show more Gaussian characteristics, which is shown in Fig. 2. Conversely, while decreasing the f parameter, it would induce more linear characteristics appearing in edges of profiles, which are shown in Figs. 3, 4. This phenomenon can be also explained in analytical aspects. By expanding the error functions in to power series [21]

$$\mathrm{erf}(x) = \frac{2}{\sqrt{\pi}} \sum_{k=1}^{\infty} (-1)^{k+1} \frac{x^{2k-1}}{(2k-1)\,(k-1)!}, \tag{29}$$

Eqs. (23) and (25) can be respectively rewritten into the following

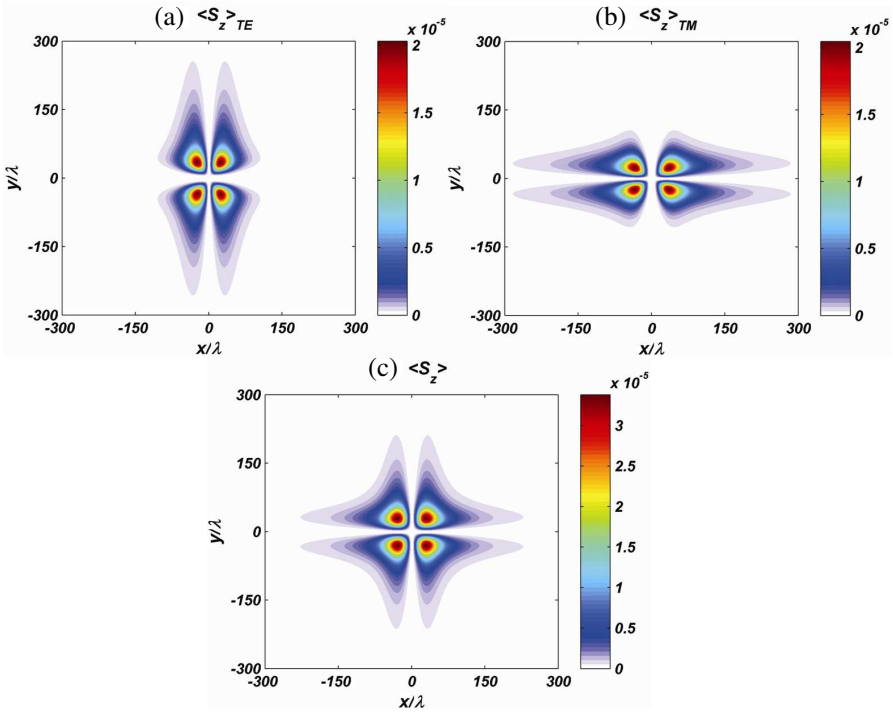

Figure 4. Energy flux distributions of the PFG beam at the plane $z = 500\lambda$, beam parameter $f = 0.03$. (a) TE term. (b) TM term. (c) The whole beam.

forms

$$\langle S_z\rangle = \frac{8z}{\pi^3 f^2 \rho^2 r^3}\left(x^2+\frac{z^2}{r^2}y^2\right)\exp\left(-\frac{\rho^2}{2f^2r^2}\right)\times L\left(k_1,x,r\right)\times L\left(k_2,y,r\right), \quad (30)$$

$$\langle S_z\rangle_p = \frac{8}{\pi^3 f^2 z^2}\exp\left(-\frac{\rho^2}{2f^2z^2}\right)\times L\left(k_1,x,z\right)\times L\left(k_2,y,z\right), \quad (31)$$

where the factor $L(k_j, u, l)$ in Eqs. (30) and (31) is represented by

$$L\left(k_j,u,l\right) = \left\{\sum_{k_j=1}^{\infty}\left(-1\right)^{2k_j+1}\frac{\left(\frac{x}{2fl}\right)^{2k_j-1}}{\left(2k_j-1\right)\left(k_j-1\right)!}\right\}^2, \quad (j=1,2;\ \ u=x,y;\ \ l=r,z), \quad (32)$$

Observing Eqs. (30) and (31), it is found that, the total energy flux distributions of the PFG beam can be represented by the product

of Gaussian parts and sums of linear combinations with respect to powers of x and y. Therefore, the decrement of the f parameter would simultaneously induce the decrement of Gaussian parts and the increment of the linear combined factor L. As a result, the edges of profiles show more linear characteristics in Figs. 3, 4.

Figure 5 shows comparisons of the total energy flux distributions between the paraxial and non-paraxial cases, for different values of the f parameter. Among these subfigures, (a), (c) and (e) are calculated by Eq. (23). Comparably, (b), (d) and (f) are calculated by Eq. (25). One can conclude from these contour plots that, when $f = 0.03$, the paraxial result coincides well with the non-paraxial result. Whereas, as the f parameter subsequently increases, the discrepancy between two cases begins to show up. To demonstrate this discrepancy in a more detailed approach, Figs. 6, 7 show comparisons of the normalized energy flux distributions of the PFG beam at the cross section $x = y$, for different values of the f parameter. These figures indicate that, the paraxial approximation holds true if the f parameter is in the vicinity of or lower than 0.05. When $f > 0.05$, the discrepancy between the paraxial and non-paraxial cases turns out to be in evidence. This result corresponds well to requirements of the f parameter in Ref. [4]. Here, one can demonstrates that, while increasing the f parameter, the basic physical cause for these differences is the applications of different approximations, the method of stationary phase and the paraxial approximation, respectively. The method used in solving Eq. (17) is the method of stationary phase, which is applicable to both the paraxial and non-paraxial case. However, Eq. (25) is derived under the validation of paraxial approximation Eq. (24), which is only applicable to the paraxial case. When the value of the f parameter increases, the PFG beam is more alike a paraxial beam. Finally, the results by using two different approximations deviate from each other, which have been shown in Figs. 6, 7. Therefore, in practical applications, one can freely manipulate diffraction patterns of the PFG beam by choosing different f parameters of the initial laser source.

Figure 8 depicts the comparison between the results calculated by the direct FFT method [23–26] and the numerical result (see Eq. (23)), for different reference distances from the source plane. The f parameter is chosen as $f = 0.53$. The principle of the fast Fourier transform (FFT) method has been explicitly introduced in Refs. [25, 26]. In our paper, we can utilize this method to directly perform the integrals in Eqs. (17) and (18) instead of using the method of stationary phase. In Fig. 8, the red line is calculated by the analytical form Eq. (23), while the blue line is directly calculated by Eqs. (17) and (18) by using the FFT method. From comparisons of two lines, one can observe

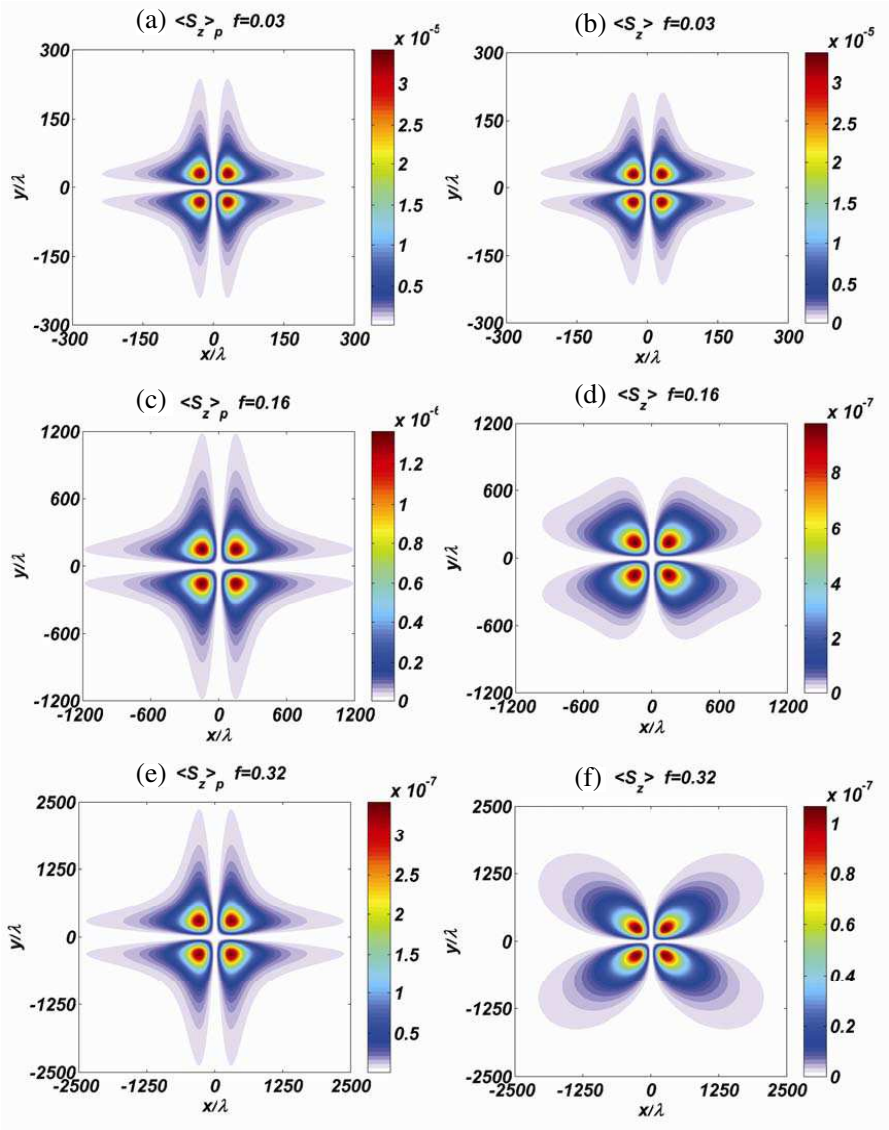

Figure 5. Comparisons of the total energy flux distributions between the paraxial and non-paraxial cases, at the plane $z = 500\lambda$, for different values of the f parameter. (a), (c), (e): paraxial result (calculated by Eq. (25)). (b), (d), (f): non-paraxial result (calculated by Eq. (23)).

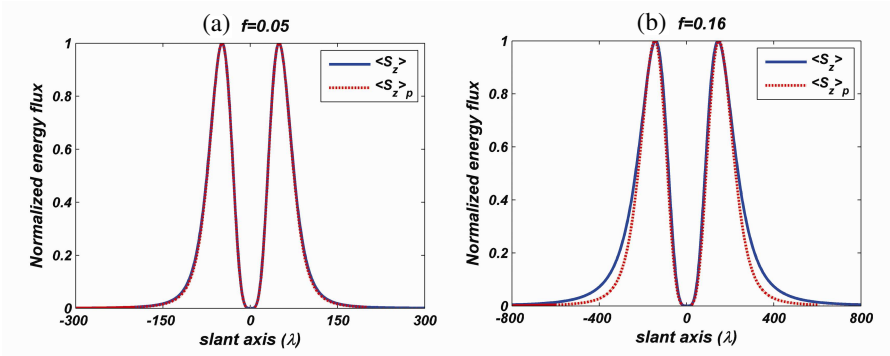

Figure 6. Comparisons of the normalized transversal energy flux distributions (cross section $x = y$) between the paraxial and non-paraxial cases, at the plane $z = 500\lambda$. (a) $f = 0.05$, (b) $f = 0.16$.

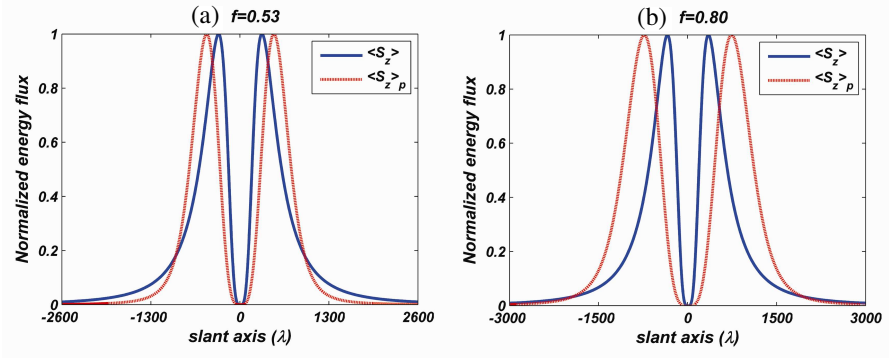

Figure 7. Comparisons of the normalized transversal energy flux distributions (cross section $x = y$) between the paraxial and non-paraxial cases, at the plane $z = 500\lambda$. (a) $f = 0.53$, (b) $f = 0.80$.

that, in the far field ($z = 500\lambda$), the result by using the FFT method corresponds well with that by utilizing the method of stationary phase, which confirms that the utilization of the method of stationary phase is valid in our paper. However, in the short distance depart from the source ($z = 50\lambda$), results calculated by two methods can not match with each other. This is because in short distances, the evanescent wave play a major role in the diffracted wave field, thus, the result directly calculated by Eqs. (17), (18) is more precise than that calculated by Eq. (23).

Figure 9 shows the comparison between the energy density $W(\hat{\mathbf{r}}) = E(\hat{\mathbf{r}}) + H(\hat{\mathbf{r}})$ and the energy flux $\langle S_z \rangle$ at the reference plane $z = 500\lambda$. The distributions of the energy and the energy flux are both normalized to their maximal values, respectively. Fig. 9 indicates that, in the far field, distributions of the energy density and energy flux gradually differ in their patterns when the f parameter increases from 0.08 to 0.53. This is because, at large f-value, the z component of the diffracted field hardly exists; the transversal electric/magnetic components play major roles in distributions of the energy density (flux). Therefore,

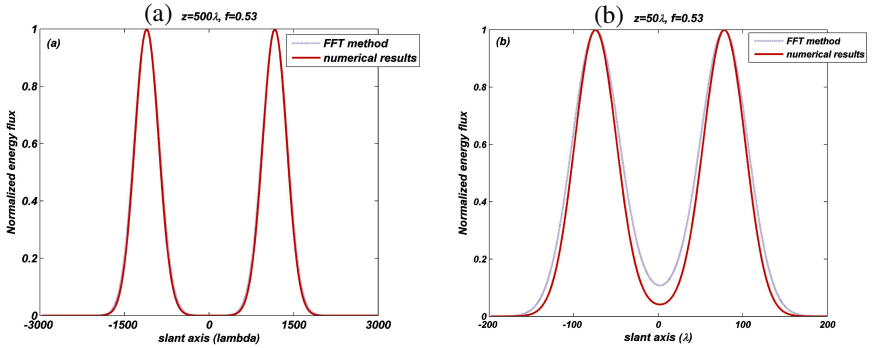

Figure 8. Comparison between the results calculated by the direct FFT method (the blue line) and the numerical result (the red line). The f parameter is chosen as $f = 0.53$. (a) $z = 500\lambda$, (b) $z = 50\lambda$.

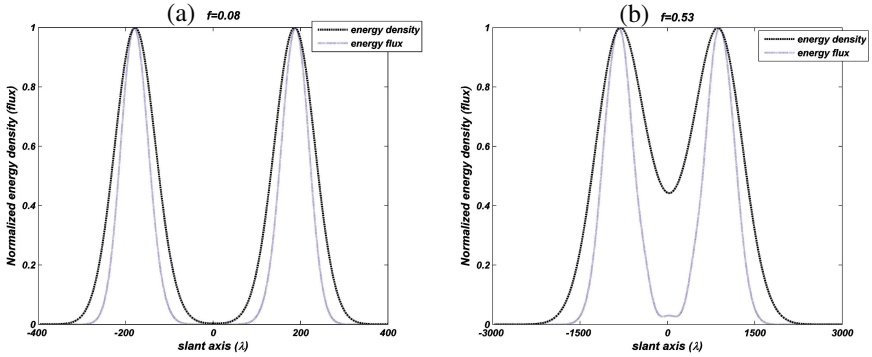

Figure 9. Comparisons between the energy density $W(\hat{\mathbf{r}}) = E(\hat{\mathbf{r}}) + H(\hat{\mathbf{r}})$ and the energy flux $\langle S_z \rangle$ of the PFG beam, for different values of the f parameter. The diffraction distance is chosen as $z = 500\lambda$. (a) $f = 0.08$, (b) $f = 0.53$.

the value of the z component of the time-averaged Poynting vector is smaller than that of the transversal energy density vectors.

Finally, our vectorial results such as Eqs. (21)–(24) can be compared with some scalar cases (see Refs. [3–5]). Observing Figs. 1–3 of Ref. [4], one can conclude that, the intensity of scalar PFG beams for both the paraxial and non-paraxial cases are continually distributed in the transversal plane upon propagation. However, in our numerical examples such as Figs. 2–5 illustrate, for the vectorial case, there exist phase singularity in the cross-section $x = 0$ and $y = 0$ due to the effect of phase flip in the source plane. This means that the energy flux distributions for the vectorial case (polarized along the x axis) are not continually distributed in the transversal plane. This difference between the vectorial theoretical case and the scalar theoretical case not only exists under the paraxial approximation, but also are applicable for the non-paraxial case. As we know, this difference has not been introduced in previous reports such as [3–5].

5. CONCLUSIONS

In this paper, based on the vectorial angular spectrum representation and the method of stationary phase, internal vectorial structures of the phase-flipped Gauss (PFG) beam in the far field are derived in analytical forms. Energy flux distributions for the TE term, TM term and the whole beam are depicted by numerical examples. Influences of the f parameter on the energy flux distributions are analyzed in a detailed approach. Besides, discrepancies of the total energy flux distributions between the paraxial and non-paraxial results are illustrated and analyzed by expansions of the error function into power series. It is found that, for the PFG beam diffracting in free space, the paraxial approximation holds true if the f parameter is in the vicinity of or lower than 0.05. These results may provide potential applications for productions and manipulations of the PFG beam in free space optical communications.

ACKNOWLEDGMENT

This work is supported by the National High Tech Research and Development Program of China (2007AA04Z181), partially supported by the National Natural Science Foundation of China (61077012), the NUST Research Funding No. 2010ZYTS031 and the Excellent Doctorial Candidate Training Funding in NUST. Authors of this paper are indebted to the reviewers for their invaluable comments and suggestions.

REFERENCES

1. Delaubert, V., D. A. Shaddock, P. K. Lam, B. C. Buchler, H. Bachor, and D. E. McClelland, "Generation of a phase-flipped Gaussian mode for optical measurements," *J. Opt. A: Pure Appl. Opt.*, Vol. 4, 393–399, 2002.
2. Treps, N., U. Andersen, B. Buchler, P. K. Lam, A. Maitre, H. Bachor, and C. Fabre, "Surpassing the standard quantum limit for optical imaging using nonclassical multimode light," *Phys. Rev. Lett.*, Vol. 20, 203601, 2002.
3. Banerji, J., "Propagation of a phase flipped Gaussian beam through a paraxial optical ABCD system," *Opt. Commun.*, Vol. 258, 1–8, 2006.
4. Gao, Z. and B. Lü, "Non-paraxial propagation of phase-flipped Gaussian beams," *Chin. Phys. B*, Vol. 17, 943–949, 2008.
5. Gao, Z. and B. Lü, "Phase-flipped Hermite-Gaussian beams and their propagation beyond the paraxial approximation," *Opt. Commun.*, Vol. 279, 130–140, 2007.
6. Herrero, R. M., P. M. Mejias, S. Bosch, and A. Carnicer, "Vectorial structure of non-paraxial electromagnetic beams," *J. Opt. Soc. Am. A*, Vol. 18, 1678–1680, 2001.
7. Mejias, P. M., R. M. Herrero, G. Piquero, and J. M. Movilla, "Parametric characterization of the spatial structure of non-uniformly polarized laser beams," *Prog. Quantum Electron.*, Vol. 26, 65–130, 2002.
8. Guo, H., J. Chen, and S. Zhuang, "Vector plane wave spectrum of an arbitrary polarized electromagnetic wave," *Opt. Express*, Vol. 14, 2095–2100, 2006.
9. Zhou, G., "Analytical vectorial structure of Laguerre-Gaussian beam in the far field," *Opt. Lett.*, Vol. 31, 2616–2618, 2006.
10. Deng, D. and Q. Guo, "Analytical vectorial structure of radially polarized light beams," *Opt. Lett.*, Vol. 32, 2711–2713, 2007.
11. Zhou, G., "Far-field structure of a linearly polarized plane wave diffracted by a rectangular aperture," *Opt. Laser Technol.*, Vol. 41, 504–508, 2009.
12. Liu, D. and Z. Zhou, "Analytical vectorial structure of the anomalous hollow beam in the far field," *Opt. Laser Technol.*, Vol. 42, 640–646, 2010.
13. Li, J., Y. Chen, Y. Xin, M. Zhou, and S. Xu, "Vectorial structural characteristics of four-petal Gaussian beams in the far field," *Eur. Phys. J. Appl. Phys.*, Vol. 50, 30702, 2010.

14. Zhou, G., "Analytical vectorial structure of controllable dark-hollow beams in the far field," *J. Opt. Soc. Am. A*, Vol. 26, 1654–1660, 2009.
15. Zhou, G. and F. Liu, "Far field structural characteristics of cosh-Gaussian beam," *Opt. Laser Technol.*, Vol. 40, 302–308, 2008.
16. Li, J., Y. Chen, S. Xu, Y. Wang, M. Zhou, Q. Zhao, Y. Xin, and F. Chen, "Analytical vectorial structure of Hermite-cosine-Gaussian beam in the far field," *Opt. Laser Technol.*, Vol. 43, 152–157, 2010.
17. Tang, H., X. Li, G. Zhou, and K. Zhu, "Vectorial structure of helical hollow Gaussian beams in the far field," *Opt. Commun.*, Vol. 282, 478–481, 2009.
18. Zhou, G. and J. Zheng, "Vectorial structure of Hermite-Laguerre-Gaussian beam in the far field," *Opt. Laser Technol.*, Vol. 40, 858–863, 2008.
19. Carter, W. H., "Electromagnetic field of a Gaussian beam with an elliptical cross section," *J. Opt. Soc. Am.*, Vol. 62, 1195–1201, 1972.
20. Mandel, L. and E. Wolf, *Optical Coherence and Quantum Optics*, Cambridge U. Press, Cambridge, 1995.
21. Abramowitz, M. and I. A. Stegun, *Handbook of Mathematical Functions*, Dover, 1972.
22. Nemoto, S., "Nonparaxial Gaussian beams," *Appl. Opt.*, Vol. 29, 1940–1946, 1990.
23. Mansuripur, M., "Distribution of light at and near the focus of high-numerical-aperture objectives," *J. Opt. Soc. Am. A*, Vol. 3, 2086–2093, 1986.
24. Rohrbach, A. and E. H. K. Stelzer, "Trapping forces, force constants, and potential depths for dielectric spheres in the presence of spherical aberrations," *Appl. Opt.*, Vol. 41, 2494–2507, 2002.
25. Leutenegger, M., R. Rao, R. A. Leitgeb, and T. Lasser, "Fast focus field calculations," *Opt. Express*, Vol. 14, 11277–11291, 2006.
26. Boruah, B. R. and M. A. A. Neil, "Focal field computation of an arbitrary polarized beam using fast Fourier transforms," *Opt. Commun.*, Vol. 282, 4660–4667, 2009.